Ranking the Key Parameters of Immersion Precipitation Process and Modeling the Resultant Membrane Structural Evolution

M. Seifollahi Bazarjani, N. Mohammadi, S. M. Ghasemi

Loghman Fundamental Research Group, Polymer Engineering Department, Amirkabir University of Technology, Tehran, Iran

Received 23 April 2008; accepted 11 January 2009
DOI 10.1002/app.30023
Published online 14 April 2009 in Wiley InterScience (www.interscience.wiley.com).

ABSTRACT: Key parameters coupling with the instantaneous nucleation concept (ie, the Big Bang analogy) was used to model immersion precipitation process. The merits of the acquired model were verified via comparing its predictions with experimental results of two well-prepared and characterized cellulose acetate (CA) and polyacrylonitrile (PAN) membranes. A morphology predictable map, $\Delta P\eta^{-1}$ versus ϕ_1, was constructed, where ΔP, η and ϕ_1 are osmotic pressure difference between nonsolvent and dope solution, dope viscosity and intruded nonsolvent volume fraction into the dope, respectively. The phase separation map, $\Delta P\eta^{-1}$ (proportional with apparent system diffusivity with the unit of time^{-1}) versus ϕ_1 showed three regimes which, at least qualitatively, depicted the correct morphological evolution trends of the studied systems. Phase separation in regime one of CA membrane with the longest delayed time or lowest $\Delta P\eta^{-1}$, led to bead-like morphology. CA membrane with the shortest elapsed time or highest $\Delta P\eta^{-1}$, separated to finger-like morphology in regime three. Finally, phase separation in the intermediate regime of CA membrane, ended up to sponge-like morphology. Phase separation time scales of the PAN membranes versus intruded nonsolvent into the dope solution were located in finger-like region of the CA membrane, which its downward transition lowered the fingers population. © 2009 Wiley Periodicals, Inc. J Appl Polym Sci 113: 1529–1538, 2009

Key words: membrane structural evolution; immersion precipitation; polymer lean phase nucleation; modeling; osmotic pressure

INTRODUCTION

Nowadays, the preparation of asymmetric polymeric membranes through the immersion precipitation process is one of the most well-known technologically practiced fabrication methods.[1] Loeb and Sourirajan[2] pioneered a procedure for making asymmetric cellulose acetate (CA) membranes. Later, it was facilitated by casting a new formulation containing 25 wt % of cellulose acetate, 30 wt % of formamide, and 45 wt % of acetone at room temperature and its direct immersion into nonsolvent.[3] After this finding, several research groups[4–7] investigated the effects of different effective variables, such as casting solution composition, evaporation time, and coagulation bath temperature on membranes performance prepared from CA-acetone-formamide-water system. The quaternary phase diagram of the system has been determined and used to describe membrane structures and properties.[4] Statistically designed experiments also have been applied to optimize the performance of the cellulose acetate membrane by maximizing the permeate flux at equal salt rejection.[6] Membrane performances were found insensitive to variations in the evaporation time from 2 to 6 s.[6] Evaporation time effect on final membrane performance depends on the initial dope location on phase diagram of the system.[7]

Therefore, main membrane characteristics, namely morphology and performance, can be designed by manipulating many effective material and process based parameters.[8] Design guidelines toward membrane performance via its relationship with formed structure have been set as an elusive goal by many research groups.[9–18] Basically, any structure evolution specifically in polymers is mainly governed by the time scale of material dynamics normalized by the special process time scale referred generally to the Deborah number.[19] Looking for the time scale of phase separation in a polymer solution during immersion precipitation, Yilmaz and McHugh[9] inferred the slope of tie lines as the key governing parameter. McHugh and coworkers[9,10] did mathematical modeling to figure out the role of phase separation path on structure evolution and were able to predict the time scale of turbidity development for some solutions. Their approach, however, required several diffusion coefficients and interaction parameters for exact solution of all the involved equations. These parameters, specifically their concentration

Correspondence to: N. Mohammadi (mohamadi@aut.ac.ir).

dependence, were either not available or multiple data could be found for every system, making model reliability as a predictive tool questionable. Complementing McHugh's research group activities in membrane structure prediction, Smolders et al.[11] found instantaneous and delayed demixing as prerequisites to the finger-like and sponge-like structures formation, respectively. Later, the correlation; $K = C\gamma^n$ among the precipitant volume (γ), polymer concentration (C), and precipitation rate of casting solution, K, after its immersion into nonsolvent bath, were reported where n represented the interaction parameter between the polymer and the solvent.[12] Although high n values were mentioned for achieving membranes with a fine porous structure, the critical n value for morphology transition was not quantified.[12] Miscibility gap has been also introduced as a criterion for membrane morphology prediction and quantified by the following equation[13]:

$$\Phi = \frac{\Delta\delta_{p-s}\Delta\delta_{p-\mathrm{ns}}}{\delta_p\Delta\delta_{s-\mathrm{ns}}} \quad (1)$$

where $\Delta\delta_{p\text{-}s}$, $\Delta\delta_{p\text{-ns}}$, and $\Delta\delta_{s\text{-ns}}$ are the solubility differences between polymer–solvent, polymer–nonsolvent, and solvent–nonsolvent, respectively, whereas δ_p is polymer solubility parameter. Miscibility gap increase or Φ decrease enhances the probability of sponge-like morphology formation and vice versa.

The role of solution phase separation time scale on morphology development in immersion precipitation process is mainly attributed to the energy barriers against nucleation. Quite recently, the nucleation time scale dependence on system location on the phase diagram was confirmed.[20,21] The relaxation time scale decay has been observed by directing phase separation path toward spinodal boundaries. In addition, several simple criteria, ie, membrane final thickness, turbidity, porosity and pure water permeability, have been introduced for quantifying phase separation path in membrane formation.[14,15] The prediction of membrane structure and corresponding performances based on thermodynamic and kinetic parameters, however, was mentioned as yet to be solved.[14,15] Polymer-rich phase glassification during phase separation has been demonstrated as the required condition for morphology stabilization.[16] The balance between local volumetric rates of solvent–nonsolvent exchange with the vitrification rate was suggested as the key factor governing growth or suppression of macrovoids.[17] Finally, threshold elasticity development in polymer-rich phase has been introduced as the criterion of halting phase separation and stabilizing membrane structure.[18] In other words, membrane formation temperature at which polymer-rich phase elastic modulus equals its loss modulus is the criterion of structure stabilization.

In this research work, a phenomenological approach was used to rank the key parameters controlling membrane morphology and performance in a model CA membrane. Then, membrane morphological evolution was modeled in analogy with the "Big Bang" concept and verified by the characteristics of CA and polyacrylonitrile (PAN) model membranes.

EXPERIMENTAL

Materials

CA with acetyl content of 39.8 wt %, M_w = 30,000 g/mol, density of 1.39 g/cm^3 and purity of more than 99% was purchased from Sigma-Aldrich (St. Louis, MO). Poly(acrylonitrile-*co*-methylacrylate), PAN, with composition of 94/6 wt %, M_v = 70,000 g/mol and PDI = 3.2 were from Polyacryl (Tehran, Iran). Acetone, formic acid, dimethyl formamide (DMF), and formamide were all supplied by Merck (Whitehouse Station, NJ) and used as received. Tap water was used as the coagulant.

Preparation and rheological characterization of polymer solutions

Polymer solutions containing 25 wt % of the CA in mixed solvents with various formamide to acetone (FA) weight ratios (x) were prepared and denoted by CA-FAx, x was 0, 0.2, 0.25, 0.33, 0.5, 0.67, and 1 in different dope solutions. PAN solutions containing 10 wt % of the PAN in pure DMF (denoted by D) or mixed solvents with formamide (denoted by F) or formic acid (denoted by FO) to DMF weight ratios of 0.167 were prepared and designated by PAN-FD0.0, PAN-FD0.167 and PAN-FOD0.167, respectively. A Brookfield viscometer (model RVT-ESER: 55,162) was used to determine the zero shear viscosity of polymer solutions at 20°C.

Membrane preparation

Each polymer solution was cast as a thin film, 200 μm in thickness, on 280 × 300 mm^2 smooth glass. The membrane precursor then, was quickly immersed into a vessel containing 6 L of stagnant tap water at 20°C and left for at least 15 min. Subsequently, the sample was transferred into a vessel with larger volume containing tap water and left for a week before conducting any characterization on the membrane.

Pure water permeability

A dead-end standard stirred test cell apparatus was used to measure the pure water permeability of membrane under 5 atmosphere of nitrogen gas

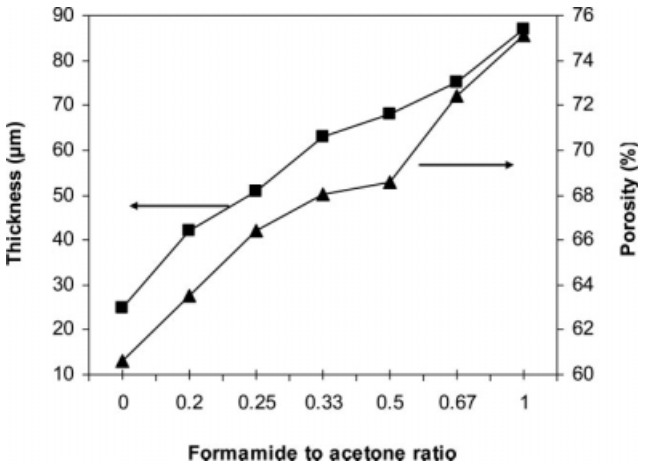

Figure 1 Thickness and porosity of the CA membranes versus their FA ratios (by weight) in the casting solutions. The initial thickness of the casting solution layer was 200 μm.

pressure.[22] The membrane sheets were cut into circles, 6.5 cm in diameter before use. Each measurement was repeated on five replicas and the average values were reported.

Turbidimetry

Membrane turbidity was measured by a turbidimeter (model 2001N Hach). For each membrane, at least three replicates were put in the turbidimeter cell and characterized. The average value was reported for each sample.

Porosimetry

Each membrane was taken out of tap water, surface dried, and weighed (X_1). It was then transferred to 60°C vacuum oven and left for 24 h to remove its trapped and free water. Later, the membrane was weighed again (X_2) and its porosity was calculated by the use of eq. (2):

$$\text{Porosity } (\%) = \frac{(1 - X_2 X_1^{-1})\rho_p}{X_2 X_1^{-1}(1 - \rho_p) + \rho_p} \times 100 \qquad (2)$$

where ρ_p (g/cm^3) is polymer density. Equation (2) has been derived from the traditional porosimetry equation based on volume measurement[23]:

$$\text{Porosity } (\%) = \frac{V_{\text{void}}}{V_{\text{total}}} \times 100 = \frac{V_{\text{total}} - V_{\text{polymer}}}{V_{\text{total}}} \times 100 \qquad (3)$$

Scanning electron microscopy

Each membrane was freeze-dried and fractured in liquid nitrogen. Then, its cross-section was coated with a thin layer of gold and examined with a scanning electron microscope (SEM; model E382, Herisau Schweiz).[23]

RESULTS AND DISCUSSION

Figure 1 shows membrane thickness and porosity versus the FA ratio in the CA casting solutions. The increase in FA ratio enhanced membrane thickness monotonically, whereas a short plateau was observed in porosity increase. An increase in FA ratio up to 0.33 did not lead to measurable permeability, whereas it increased membrane turbidity to a maximum (Fig. 2). By crossing a FA ratio of 0.33, a severe membrane turbidity decrease and permeability increase were observed (Fig. 2). Major turbidity and permeability changed right at the plateau region of porosity versus FA ratio was attributed to a transition in membrane void structure without changing its overall porosity. Membrane performance depends on overall porosity, void average size, and morphology dictated by various evolution paths followed on system phase diagram (Fig. 3). Phase separation path one for the CA solution in acetone exposed to water led to the direct gelation of casting solution through one phase region with compact morphology and transparent membrane with negligible pure water permeability. The observed morphology occurred due to high solvent outflow and low nonsolvent inflow, leading to strong film shrinkage.[15] By changing the phase separation paths to two and three via a FA ratio increase (larger two phase region), one-phase casting solutions crossed the binodal boundary and phase separated to polymer lean and rich phases with void-matrix structure. Further, the FA ratio increase changed membrane morphology to the co-continuous void-matrix structure, by following phase separation via path four. Finally, casting solution with FA ratio corresponding phase separation via path five might nucleate through

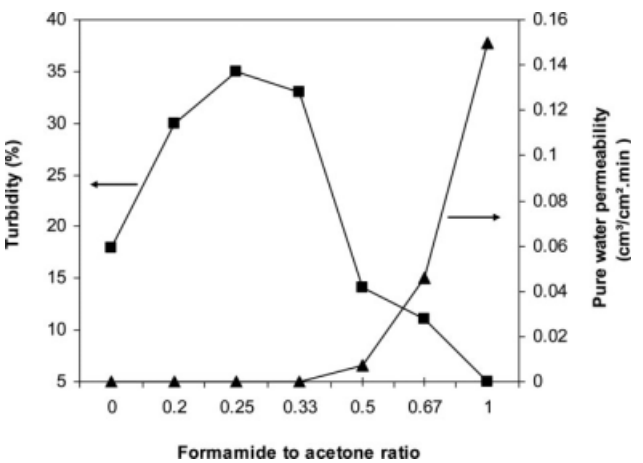

Figure 2 Turbidity and pure water permeability of the CA membranes versus FA ratios (by weight) in the casting solutions. The initial thickness of the casting solution layer was 200 μm.

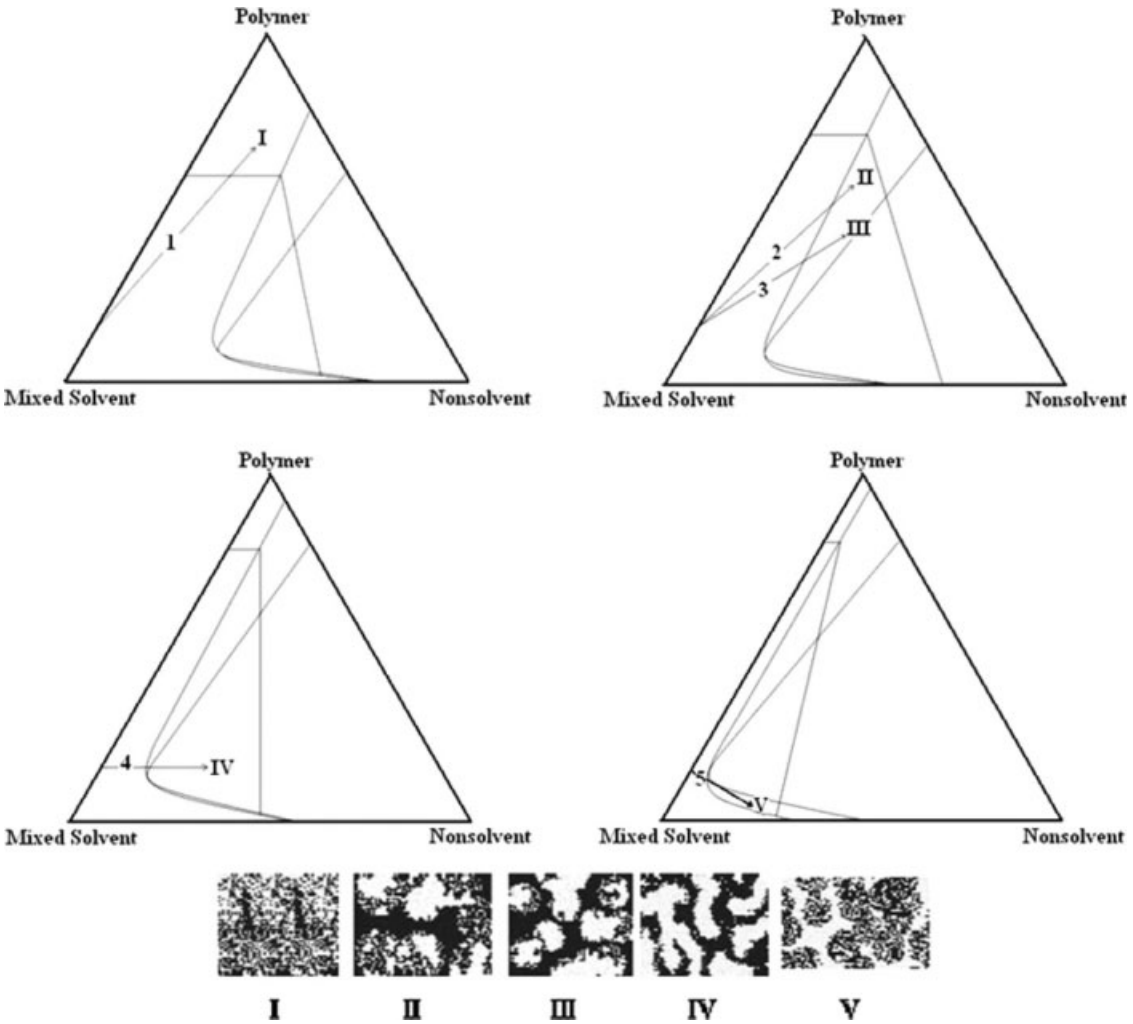

Figure 3 Phase separation paths variation in the membrane formation process via changing mixed solvent composition: paths 1–5 lead to one phase gel region, I; slow nucleation, and growth of polymer lean phase, II; faster nucleation and growth of polymer lean phase, III; spinodal decomposition, IV; and nucleation and growth of polymer-rich phase, V, respectively.

polymer-rich phase and lead to partially sintered nanometer-sized beads.

Cross-sectional morphologies of the as-prepared CA membranes are shown in Figure 4. Lower-magnification (500) pictures also are presented as an inset in every micrograph of Figure 4. The prepared CA-FA0 sample via phase separation through path one showed many mono-dispersed micron size voids containing aggregated nanovoids, Figure 4(a). The addition of the FA ratio of the CA casting solution to 0.2, however, changed phase separation path toward binodal boundary, leading to finger formation at the surface and underneath void size increase and intervoid ligament thickness decrease [Fig. 4(b)]. Phase separation of dope solutions with FA ratios of 0.25 and 0.33 via binodal region of phase diagram increased underneath void average size while changing their ligament structure to nanometer size-aggregated dense particles [Fig. 4(c,d)], respectively. The underneath cross-section of sample CA-FA0.33 appeared collapsed compared with sample CA-FA0.25 whereas their surfaces still showed finger-like structuring. The sample with a FA ratio of 0.5, however, showed interconnected (taking path four for phase separation) smaller voids with ligaments still made of aggregated dense nanoparticles without any fingering. By moving to sample CA-FA0.67, an almost-similar structure to sample CA-FA0.5 was observed except with thinner intervoid ligaments. Finally, a FA ratio of 1 led to a severe nucleation mechanism change from liquid–liquid demixing to solid–liquid demixing, with partially sintered nano-size particle structure with the highest permeability. Void size and particle size reduction in transition from sample CA-FA0.2 to CA-FA0.67 and finally to CA-FA1 was consistent with the Gibbs theory,[24,25] delineating nucleus size decrease by moving from a metastable boundary toward an unstable one

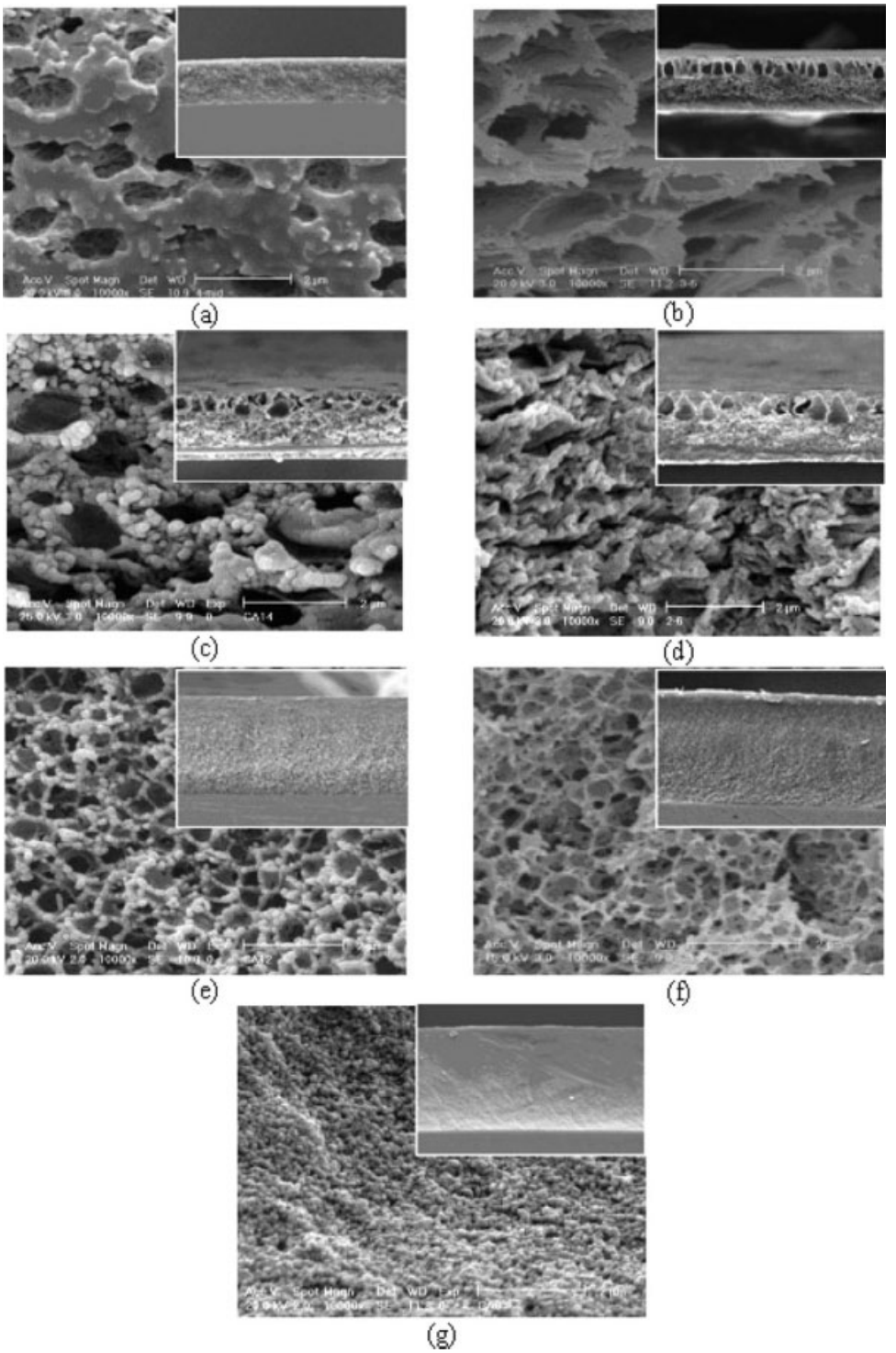

Figure 4 Scanning electron micrographs of cross section of the CA membranes prepared with different FA ratios in their casting solutions: (a) CA-FA0; (b) CA-FA0.20; (c) CA-FA0.25; (d) CA-FA0.33; (e) CA-FA0.50; (f) CA-FA0.67; and (g) CA-FA1 (×10,000 magnifications and ×500 for inset images). The initial thickness of the casting solution layer was 200 μm.

(Fig. 3). Phase separation path change should also reduce work of nucleus formation, the number of nuclei increase, and their aggregation mainly based on free energy minimization.

FA ratio enhancement in the CA casting solution increased its mixed solvents solubility parameter (Table I) and reduced their solubility difference with the nonsolvent (water) (Fig. 5). calculated by the following formula:

$$\Delta\delta_{i-j} = \left(\left(\delta_{h,i} - \delta_{h,j}\right)^2 + \left(\delta_{d,i} - \delta_{d,j}\right)^2 + \left(\delta_{p,i} - \delta_{p,j}\right)^2\right)^{\frac{1}{2}} \quad (4)$$

TABLE I
Material Parameters Used in Solubility and Mixing ΔG Calculations[a26–31]

	δ_d $(J/cm^3)^{1/2}$	δ_p $(J/cm^3)^{1/2}$	δ_h $(J/cm^3)^{1/2}$	$\delta(298)$ $(J/cm^3)^{1/2}$	ρ^* (g/cm^3)	α $(10^{-4}\ K^{-1})$	$N_{Av}\upsilon$ (cm^3/mol)
Acetone	15.5	10.4	7.0	19.94	1.147	13.0	50.57
Cellulose acetate	18.6	12.7	11.0	25.06	1.764	8.0	163.27
Dimethyl formamide	16.1	13.7	11.2	23.92	1.282	10.0	57.04
Formamide	17.2	26.2	19.0	36.65	1.460	9.0	30.83
Formic acid	14.3	11.9	16.6	24.93	1.648	11.0	27.91
Polyacrylonitrile[b]	21.7	14.1	9.1	27.43	1.310	5.16	40.50
Water	15.5	16.0	42.4	47.90	1.076	3.0	16.73

[a] ρ^* and α of material, except polymer, calculated from the density data reported in Ref. 29.
[b] ρ^* and α of polyacrylonitrile were taken from SAN40 in Ref. 31.

where δ_d, δ_p, and δ_h represent the dispersion, polar, and hydrogen bonding components of the solubility parameter, respectively. Thermodynamic affinity increase of the casting solution toward nonsolvent leads to greater nonsolvent inflow and solvent outflow. Therefore, one can write:

Solvent outflow and nonsolvent inflow

$$\propto (\Delta\delta_{ms-ns})^{-1} \quad (5)$$

In addition, solvent outflow is diminished by solubility difference decrease between polymer and mixed solvents.

$$\text{Solvent outflow } \propto (\Delta\delta_{p-ms}) \quad (6)$$

Therefore, solvent outflow is approximated by:

$$\text{Solvent outflow} \propto \frac{\Delta\delta_{p-ms}}{\Delta\delta_{ms-ns}} \quad (7)$$

Nonsolvent inflow reduced casting solution stability caused by the Gibbs free energy increase, leading to affinity decrease to more nonsolvent intrusion. Therefore, nonsolvent affinity toward casting solution should scale the reciprocal of its ΔG difference in two states; namely nonsolvent/casting solution, ΔG_1, with nonsolvent/casting solution containing intruded nonsolvent, ΔG_2:

$$\text{Nonsolvent inflow} \propto (\Delta G_2 - \Delta G_1)^{-1} \quad (8)$$

A simple equation of state based model for calculating the free energy change of mixing compressible multicomponent systems per unit volume, Δg_{mix}, has been introduced[32]:

$$\Delta g_{mix} = \left(g - g^{**}_{ref}\right) = RT \sum_i^p \frac{\phi_i \tilde{\rho}_i}{N_i v_i} \ln(\phi_i) + \sum_i^p \sum_j^p -\phi_j \tilde{\rho}_j \phi_i \tilde{\rho}_i \delta_{i,0} \delta_{j,0} + \sum_i^p \phi_i \tilde{\rho}_i^2 \delta_{i,0}^2 \quad (9)$$

where R and T are gas constant and absolute temperature, respectively. ϕ_i is the volume fraction of component I, and $\tilde{\rho}_i$ is reduced density, which is simply a measure of fractional occupied volume defined as[32]:

$$\rho_i(T) = \rho_i^* \exp(-\alpha_i T) \quad (10)$$

where α_i is the coefficient of thermal expansion for component i, ρ_i^* is the hard core density of component i, δ_{i0}^2 and δ_i^2 are the cohesive energy densities of component i in hard core state and temperature T, respectively. The calculated increase in CA solution Gibbs free energy as a function of intruded water volume fraction is shown in Figure 6. The parameters of various components used for calculations are listed in Table I. FA ratio enhancement in CA casting solution increased its affinity toward nonsolvent, ΔG difference decrease [eq. (8)]. This trend also corresponded with the observed morphological development paths in the prepared membranes, Figure 3.

The effect of polymer solution viscosity on membrane structural evolution was also considered. The zero shear viscosity of CA solution increased by FA

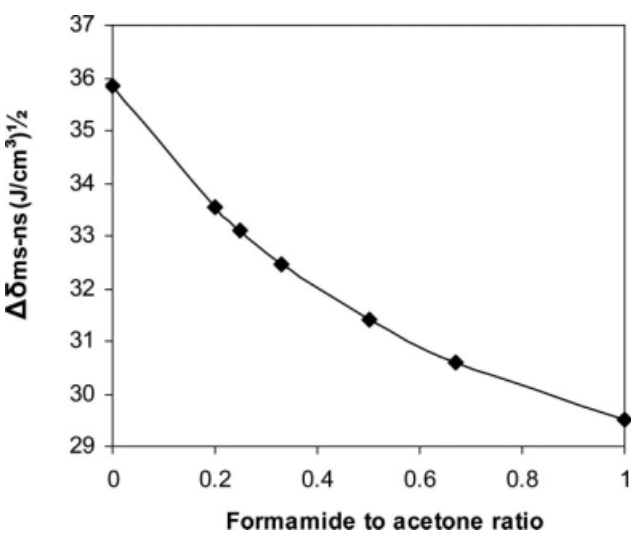

Figure 5 Solubility difference between mixed solvents-nonsolvent versus FA ratios (by weight) in casting solutions.

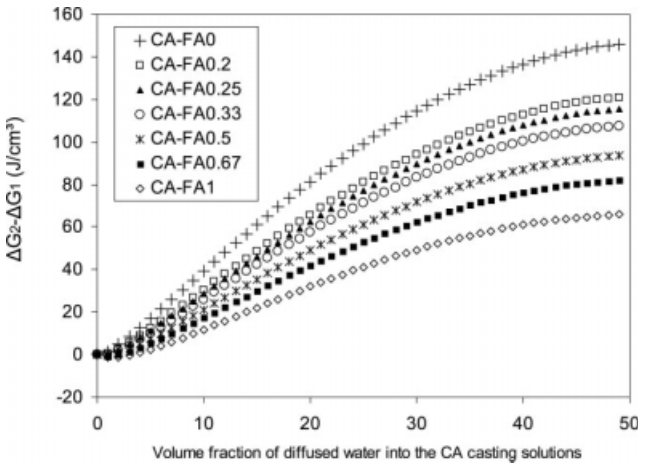

Figure 6 Gibbs free energy difference of the CA cast film as a result of intruded nonsolvent volume fraction at different FA ratios (by weight).

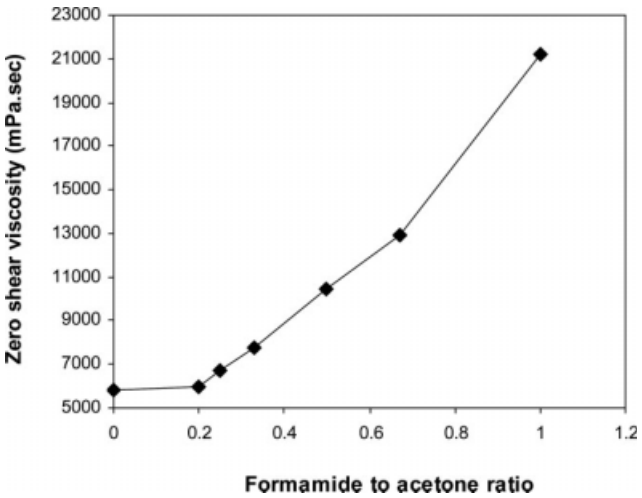

Figure 7 Zero shear viscosity of the CA casting solutions versus their FA ratios (by weight).

ratio enhancement, Figure 7. The rate of solvent outflow and nonsolvent inflow from and into the casting solution are then reduced rheologically by FA ratio enhancement. Therefore, solvent outflow to nonsolvent inflow ratio depends also on dimensionless nonsolvent to solution viscosities:

$$\xi \propto \frac{\eta_{\text{nonsolvent}}}{\eta_{\text{solution}}} \tag{11}$$

Combining eqs. (7), (8), and (11), one may write the following correlation:

$$\xi = \text{Solvent outflow /Nonsolvent Inflow}$$

$$\propto \left[\frac{(\Delta G_2 - \Delta G_1)}{RT}\frac{\eta_{\text{ns}}}{\eta_{\text{sol}}}\frac{\Delta\delta_{p-\text{ms}}}{\Delta\delta_{\text{ms}-\text{ns}}}\right] \tag{12}$$

The ΔG difference was normalized by RT to make it dimensionless as other effective parameters. Closer inspection of eq. (12) implies that higher ξ leads to lower porosity and thinner membranes. Therefore, one may write the following correlation between membrane thickness, porosity and ξ^{-1}:

(Thickness) and (Porosity)

$$\propto \left[\frac{RT}{(\Delta G_2 - \Delta G_1)}\frac{\eta_{\text{sol}}}{\eta_{\text{ns}}}\frac{\Delta\delta_{\text{ms}-\text{ns}}}{\Delta\delta_{p-\text{ms}}}\right] \tag{13}$$

Or

$$(\text{Thickness})\text{and}(\text{Porosity}) = K \times \left(\frac{RT}{(\Delta G_2 - \Delta G_1)}\right)^A \times \left(\frac{\eta_{\text{sol}}}{\eta_{\text{ns}}}\right)^B \left(\frac{\Delta\delta_{\text{ms}-\text{ns}}}{\Delta\delta_{p-\text{ms}}}\right)^C \tag{14}$$

where K, A, B, and C are adjustable parameters. For sake of brevity, we calculated the adjustable parameters based on porosity data.

The calculated K, A, B, and C for different amounts of intruded nonsolvents are presented in Table II. A, B, and C powers represent the relative importance of each parameter contribution in membrane formation. The highest values of B in rows with intruded water volume fractions up to 10 vol % imply the dominated role of solution viscosity whereas C or representative of thermodynamic affinity takes the second ranking. Water intrusion greater than 10 vol % leads to A as the first ranking and B as the second one. Therefore, the key affecting parameters of membrane morphological evolution in the CA casting solutions are dope solution viscosity and thermodynamic affinity toward nonsolvent respectively up to 10 vol % of nonsolvent intrusion. For the CA casting solutions containing higher amounts of intruded nonsolvent, ΔG difference and solution viscosity take the first and second ranking, respectively. It should be emphasized that for less than 10 vol % of nonsolvent intrusion into dope solution, Ruaan's simple parameter[13] ($\Delta\delta_{p-\text{ms}}/\Delta\delta_{\text{ms}-\text{ns}}$) satisfies the estimation of the thermodynamic affinity between dope solution and nonsolvent.

TABLE II
Calculated Adjustable Parameters Based on Intruded Nonsolvent Volume Fraction into the Casting Solution

Water volume fraction	K	A	B	C
1	9.27	0.0041	0.1924	0.0983
2	9.59	0.0047	0.1857	0.1103
6	10.06	0.0207	0.1719	0.1117
10	12.79	0.0798	0.1210	0.0940
14	14.02	0.1139	0.1010	0.0844
18	14.70	0.1352	0.0913	0.0790
22	15.17	0.1499	0.0857	0.0756

Average of correlation coefficient between experimental and calculated porosity is 0.985.

On the basis of the ranked key parameters, casting solution affinity toward nonsolvent and its rheological resistance against nuclei growth were used to develop a model based on analogy with the "Big Bang" concept. Casting solution exposure to the nonsolvent leads to instantaneous nucleation of polymer lean phase where its growth against engulfing polymer rich layer determines final membrane morphology. The equation of continuity and r-component of the equation of motion in spherical coordinates are solved based on the following assumptions: (1) polymer-rich phase viscosity is greater than polymer-lean phase viscosity, (2) polymer-rich phase layer thickness is much lower than nucleus radius, (3) interfacial tension between polymer-rich and polymer-lean phases are negligible compared with other existing forces, (4) gravity is negligible and viscosity and density are constant in the nucleus clusters. Therefore, θ- and Φ-components of the velocity are zero and radial growth velocity, V_r, depends only on r. Equation of continuity become[33]:

$$\frac{1}{r^2}\frac{\partial}{\partial r}(r^2 V_r) = 0 \tag{15}$$

Hence,

$$V_r = \frac{\alpha}{r^2} \tag{16}$$

where α and r are constant parameter and nucleus radius, respectively. At nucleus surface, $r = R$, V_r is R^0. Hence,

$$V_r = R^0\left(\frac{R}{r}\right)^2 \tag{17}$$

On the other hand, momentum balance over the nucleus gives:

$$T_{rr}|_R - T_{rr}|_{R+W} = 0 \tag{18}$$

$$T_{rr} = P + \tau_{rr} \tag{19}$$

$$\tau_{rr} = -2\eta\frac{\partial V_r}{\partial r} \tag{20}$$

where T_{rr}, τ_r, P, η, and W are total force, viscous force, pressure force, viscosity of nucleus wall (polymer rich phase viscosity) and nucleus wall thickness, respectively. Combination of eqs. (17)–(20) yields:

$$R^0 = \frac{(\Delta P \times R^2)}{(12 \times \eta \times W)} \tag{21}$$

where $\Delta P(= -\Delta\mu/v_1$, -chemical potential difference/nonsolvent molar volume) is the osmotic pressure driving nucleus growth. Δμ can be calculated by taking derivative of ΔG with respect to molar volume of the nonsolvent. Taking R and W constant, R^0 is mainly quantified by $\Delta P\eta^{-1}$ with the dimension of reciprocal time that is actually structure evolution time. Interestingly, $\Delta P\eta^{-1}$ is proportional with apparent diffusivity of the system, which included not only thermodynamic motive (ΔP) for mass interchange but also considers system diffusion rate ($D \approx \eta^{-1}$).[34,35] Figure 8 shows $\Delta P\eta^{-1}$ versus the volume fraction of intruded nonsolvent into the CA casting solutions, lower part of the figure. Three regimes are distinguishable based on SEM pictures (Fig. 4). In low $\Delta P\eta^{-1}$ versus intruded water into the CA casting solutions, regime I, the membrane morphologies are bead-like. High $\Delta P\eta^{-1}$ versus intruded water into the CA casting solutions, regime III, led to membranes with finger-like morphologies at the surface. Finally, $\Delta P\eta^{-1}$ versus intruded nonsolvent in regime II ended with sponge-like morphologies. Calculated $\Delta P\eta^{-1}$ versus intruded water volume fraction into three casting solutions of PAN, PAN-FD0.0,

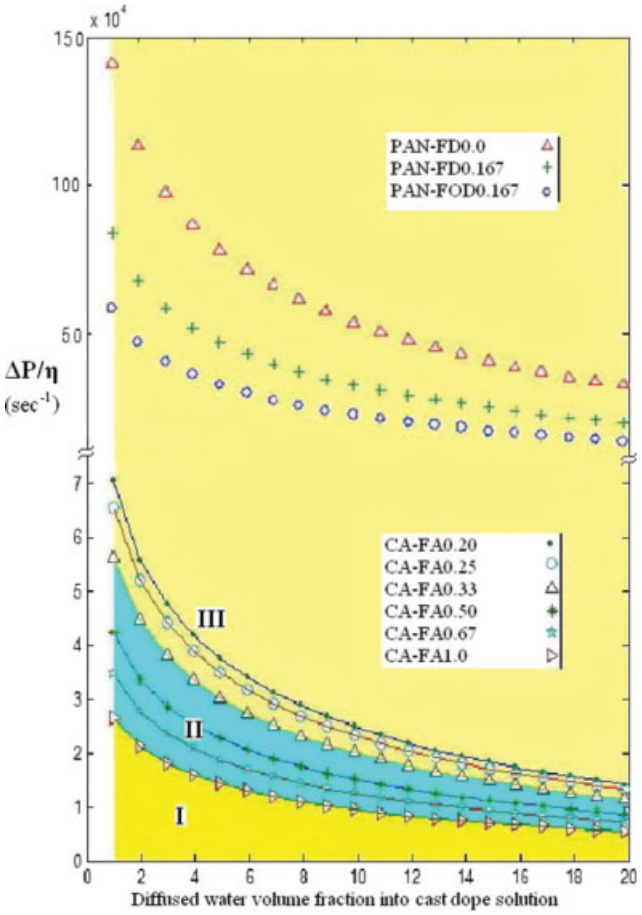

Figure 8 $\Delta P\eta^{-1}$ versus intruded water volume fraction into the casting solutions with various cosolvent to solvent compositions: CA, lower part, and PAN, upper part. The initial thickness of the casting solution layer was 200 μm. [Color figure can be viewed in the online issue, which is available at www.interscience.wiley.com.]

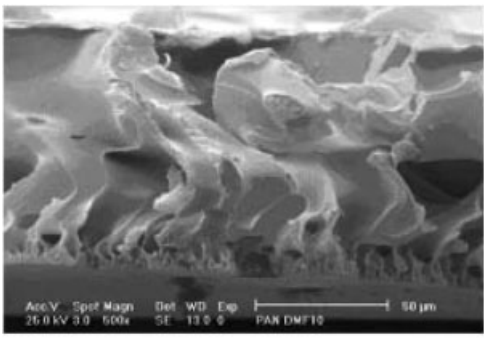

(a) PAN-FD0.0

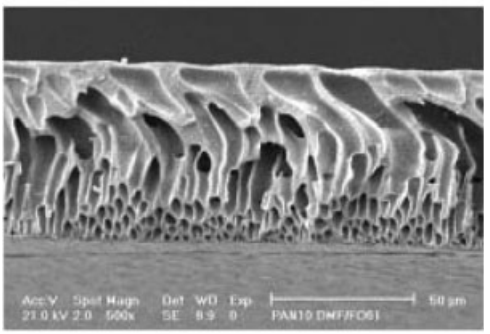

(b) PAN-FD0.167

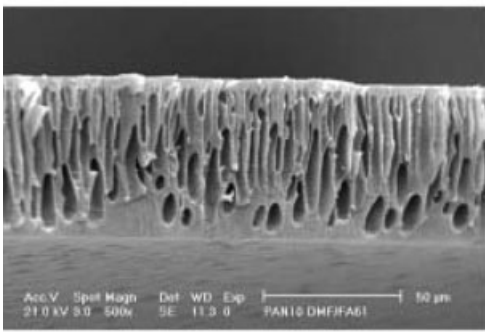

(c) PAN-FOD0.167

Figure 9 Scanning electron micrographs of cross section of the PAN based membranes: casting solutions without cosolvent, (a) with cosolvent to solvent ratio of 0.167, (b) formamide, and (c) formic acid. The initial thickness of the casting solution layer was 200 μm.

PAN-FD0.167, and PAN-FOD0.167 are also included in upper part of Figure 8. On the basis of the location of these three curves on the CA membranes map, their morphologies were expected to be finger-like. In addition, downward transition of $\Delta P\eta^{-1}$ curves versus intruded nonsolvent into the dope for various PAN membranes must lead to reduced fingering. Interestingly, the expectations were true by the inspected morphologies, Figure 9. Further experimental data points along with viscosity modification due to nonsolvent intrusion are definitely required to find out the transitional borders among different regimes. In addition, phase separation time scale might be limited by threshold polymer rich phase elasticity achievement.

It should also be noted that the aforementioned explanation is valid for constant initial thickness of casting solution which in this work was 200 μm. Initial thickness decrease, led to smaller pore size at membrane sublayer[10] and even membrane morphology transition from finger-like to sponge-like structure.[36] The $\Delta P\eta^{-1}$-based model is currently been used to include the effects of different variables, such as shear and elongational field, initial thickness of casting solution and so on, on structural evolution of membranes and fibers fabricated by immersion precipitation method. Final goal, has been establishing a simple model based on dimensionless group containing solvent-nonsolvent exchange rate (phase separation time scale), $\Delta P\eta^{-1}$, and gelation or vitrification rate.

CONCLUSIONS

A phenomenological evaluation of phase inversion process based on preparation and well-characterization of several model CA membranes led to ΔP, osmotic pressure developed by solubility difference between nonsolvent and casting solution, and casting solution viscosity as the key parameters governing structure evolution. The nucleation and growth of polymer-lean phase against polymer-rich phase in analogy with the "Big Bang" phenomenon, then, established $\Delta P\eta^{-1}$ (proportional with apparent system diffusivity) map versus intruded nonsolvent into the casting solution. For CA membranes, three regimes representing finger-like, sponge-like, and bead-like morphologies by $\Delta P\eta^{-1}$ decrease was found. Plotting $\Delta P\eta^{-1}$ versus intruded nonsolvent into the casting solutions of three PAN based model membranes agreed very well at least on trend basis with the CA based morphological evolution map.

References

1. Baker, R. W. Membrane Technology and Applications, 2nd ed.; Wiley: New York, 2004.
2. Loeb, S.; Sourirajan, S. Adv Chem Ser 1962, 38, 117.
3. Manjikian, S.; Loeb, S.; McCutchan, L. In Proceedings of First International Symposium on Water Desalination; US Department of Interior, Office of Saline Water, Washington, DC, 1965; p 159.
4. Strathmann, H.; Scheible, P.; Baker, R. W. J Appl Polym Sci 1971, 15, 811.
5. Pilon, R.; Kunst, B.; Sourirajan, S. J Appl Polym Sci 1971, 15, 1317.
6. Chian, E. S. K.; Fang, H. H. P. J Appl Polym Sci 1975, 19, 251.
7. Sirkar, K. K.; Agarwal, N. K.; Rangaiah, P. J Appl Polym Sci 1978, 22, 1919.
8. Van de Witte, P.; Dijkstra, P. J.; van den Berg, J. W. A.; Feijen, J. J Membr Sci 1996, 117, 1.
9. Yilmaz, L.; McHugh, A. J. J Appl Polym Sci 1986, 31, 997.

10. Tsay, C. S.; McHugh, A. J. J Polym Sci Part B: Polym Phys 1990, 28, 1327.
11. Smolders, C. A.; Reuvers, A. J.; Boom, R. M.; Wienk, I. M. J Membr Sci 1992, 73, 259.
12. Yanagishita, H.; Nakane, T.; Yoshitome, H. J Membr Sci 1994, 89, 215.
13. Ruaan, R. C.; Chang, T.; Wang, D. M. J Polym Sci Part B: Polym Phys 1999, 37, 1495.
14. Stropnik, C.; Musil, V.; Brumen, M. Polymer 2000, 41, 9227.
15. Stropnik, C.; Kaiser, V. Desalination 2002, 145, 1.
16. Li, S. G.; van der Boomgaard, T.; Smolders, C. A.; Strathmann, H. Macromolecules 1996, 29, 2053.
17. McKelvey, S. A.; Koros, W. J. J Membr Sci 1996, 112, 29.
18. Lin, K. Y.; Wang, D.-M.; Lai, J. Y. Macromolecules 2002, 35, 6697.
19. de Gennes, P.-G. Scaling Concepts in Polymer Physics; Cornell University Press: New York, 1991.
20. Balsara, N. P.; Rappl, T. J.; Lefebvre, A. A. J Polym Sci Part B: Polym Phys 2004, 42, 1793.
21. Lefebvre, A. A.; Lee, J. H.; Balsara, N. P.; Hammouda, B. J Chem Phys 2002, 116, 4777.
22. Ismail, A. F.; Hassan, A. R. J Membr Sci 2006, 270, 57.
23. Arbab, S.; Noorpanah, P.; Mohammadi, N.; Soleimani Kheibari, M. J Appl Polym Sci 2008, 109, 3461.
24. Kashchiev, D. Nucleation Basic Theory with Applications; Longmans and Green: New York, 2002.
25. Gibbs, J. W. On the Equilibrium of Heterogeneous Substances, Transactions of the Connecticut Academy of Science; Longmans and Green: New York, 1928; Vol. 3, p 1875.
26. Appaw, C.; Gilbert, R. D.; Khan, S. A.; Kadla, J. F. Biomacromolecules 2007, 8, 1541.
27. Stefanis, E.; Tsivintzelis, I.; Panayiotou, C. Fluid Phase Equilib 2006, 240, 144.
28. Reinert, F.; Lüthy, W. Opt Express 2005, 13, 10749.
29. Perry, R. H.; Green, D. W. Perry's Chemical Engineering Handbook; McGraw-Hill: New York, 1999.
30. Hansen, C. M. Ind Eng Chem Prod Res Dev 1969, 8, 2.
31. Ruzette, A.-V. G.; Mayes, A. M. Macromolecules 2001, 34, 1894.
32. Gonzalez-Leon, J. A.; Mayes, A. M. Macromolecules 2003, 36, 2508.
33. Bird, R. B.; Stewart, W. E.; Lightfoot, E. N. Transport Phenomena, 2nd ed.; Wiley: New York, 2002.
34. Okamoto, M.; Shiomi, K.; Inoue, T. Polymer 1995, 36, 87.
35. Vrentas, J. S.; Vrentas, C. M. J Polym Sci Part B: Polym Phys 2003, 41, 501.
36. Li, D.; Chung, T. S.; Ren, J.; Wang, R. Ind Eng Chem Res 2004, 43, 1553.